Chapter 2

Reproducibility of quantitative (*R*)-[^{11}C]verapamil studies

Daniëlle M.E. van Assema[1,2], Mark Lubberink[1,3], Ronald Boellaard[1], Robert C. Schuit[1], Albert D. Windhorst[1], Philip Scheltens[2], Bart N.M. van Berckel[1], Adriaan A. Lammertsma[1]

[1] Department of Nuclear Medicine & PET Research, VU University Medical Center, Amsterdam, The Netherlands
[2] Department of Neurology & Alzheimer Center, VU University Medical Center, Amsterdam, The Netherlands
[3] PET Centre, Uppsala University Hospital, Uppsala, Sweden

EJNMMI Research 2012;2:1.

ABSTRACT

Background: P-glycoprotein (Pgp) dysfunction may be involved in neurodegenerative diseases, such as Alzheimer's disease, and in drug resistant epilepsy. Positron emission tomography using the Pgp substrate tracer (*R*)-[^{11}C]verapamil enables *in vivo* quantification of Pgp function at the human blood-brain barrier. Knowledge of test-retest variability is important for assessing changes over time or after treatment with disease-modifying drugs. The purpose of this study was to assess reproducibility of several tracer kinetic models used for analysis of (*R*)-[^{11}C]verapamil data.

Methods: Dynamic (*R*)-[^{11}C]verapamil scans with arterial sampling were performed twice on the same day in 13 healthy controls. Data were reconstructed using both filtered back projection (FBP) and partial volume corrected ordered subset expectation maximization (PVC OSEM). All data were analyzed using single-tissue and two-tissue compartment models. Global and regional test-retest variability was determined for various outcome measures.

Results: Analysis using the Akaike information criterion showed that a constrained two-tissue compartment model provided the best fits to the data. Global test-retest variability of the volume of distribution was comparable for single-tissue (6%) and constrained two-tissue (9%) compartment models. Using a single-tissue compartment model covering the first 10 min of data yielded acceptable global test-retest variability (9%) for the outcome measure K_1. Test-retest variability of binding potential derived from the constrained two-tissue compartment model was less robust, but still acceptable (22%). Test-retest variability was comparable for PVC OSEM and FBP reconstructed data.

Conclusions: The model of choice for analysing (*R*)-[^{11}C]verapamil data is a constrained two-tissue compartment model.

INTRODUCTION

P-glycoprotein (Pgp) is considered to be the most important efflux transporter at the human blood-brain barrier (BBB), because of its high expression and its ability to transport a wide range of substrates from the brain into the circulation and cerebrospinal fluid. Pgp plays an important role in protecting the brain from endogenous and exogenous toxic substances by removing them before they reach the parenchyma [1-5]. It has been hypothesised that decreased Pgp function and/or expression at the BBB are involved in several neurological disorders, such as Creutzfeldt-Jakob disease, Parkinson's disease and Alzheimer's disease (AD) [6-9]. On the other hand, increased Pgp function may be involved in drug resistant epilepsy [10].

Over the past years several positron emission tomography (PET) tracers have been developed for quantifying Pgp function *in vivo*. Of these, (racemic) [^{11}C]verapamil, (*R*)-[^{11}C] verapamil and [^{11}C]-*N*-desmethyl-loperamide have been used in humans [8, 11-15]. Both (*R*) and (*S*) enantiomers of verapamil are substrates for Pgp, but (*R*)-[^{11}C]verapamil is the preferred isomer for quantification of Pgp function, as it is metabolized less than (*S*)-[^{11}C] verapamil [16-17]. (*R*)-[^{11}C]verapamil has been widely used both in healthy controls without [12,18-20] and with modulation of Pgp function [21-22] and in neurological diseases such as epilepsy [10], Parkinson's disease [11] and AD [9].

Several tracer kinetic models for quantification of (*R*)-[^{11}C]verapamil data have been reported [19,23] with the standard single-tissue compartment model (1T2k) being used most frequently. An alternative approach is to apply the single-tissue compartment model only to the first 10 min after injection (1T2K^{10}), in order to minimise effects of radiolabelled metabolites potentially crossing the BBB [23]. Other studies, however, have shown that a two-tissue compartment model (2T4k) provides good fits to the data, and a study using spectral analysis as well as studies in which Pgp was blocked pharmacologically suggests that indeed two compartments can be identified [9,21,23]. An important characteristic of a tracer kinetic model is its test-retest (TRT) variability. Not only does this determine group sizes in cross-sectional studies, it is also particularly important in longitudinal studies designed to assess changes over time or after treatment with disease-modifying drugs. To date, only one study has reported on TRT variability of (*R*)-[^{11}C]verapamil data [19]. This study, however, did not include all tracer kinetic models mentioned above and TRT variability was only reported for a whole brain region of interest (ROI). Clearly, information about regional TRT variability is important in order to interpret changes in Pgp function in smaller anatomical structures. Therefore, the main aim of this study was to assess regional TRT variability of (*R*)-[^{11}C]verapamil PET data for several tracer kinetic models. In addition, effects of correcting for partial volume effects on TRT variability were assessed.

MATERIALS AND METHODS

Subjects

Thirteen healthy controls, six males and seven females, were included (mean age 40 years, range 21 to 63 years). A subset of these data has been published previously as a part of the model development for (*R*)-[^{11}C]verapamil [19]. Subjects were recruited through advertisements in newspapers and by means of flyers. All subjects were screened extensively for somatic and neurological disorders and had to fulfil research diagnostic criteria for having never been mentally ill. Screening procedures included medical history, physical and neurological examinations, screening laboratory tests of blood and urine, and brain magnetic resonance imaging (MRI), which was evaluated by a neuroradiologist. Subjects were not included if there was use of drugs of abuse or use of medication known to interfere with Pgp function [24-25]. Additional exclusion criteria were history of major neurological or psychiatric illness, and clinically significant abnormalities of laboratory tests or MRI scan. Written informed consent was obtained from all subjects after a complete written and verbal description of the study. The study was approved by the Medical Ethics Review Committee of the VU University Medical Center.

MRI

Six subjects underwent a structural MRI scan using a 1.0 T Magnetom Impact scanner (Siemens Medical Solutions, Erlangen, Germany) and 7 subjects using a 1.5 T Sonata scanner (Siemens Medical Solutions, Erlangen, Germany). The scanning protocol on both scanners included an identical coronal T1-weighted 3-D MPRAGE sequence (magnetization prepared rapid acquisition gradient echo; slice thickness = 1.5 mm; 160 slices; matrix size = 256 x 256; voxel size = 1 x 1 x 1.5 mm; echo time = 3.97 ms; repetition time = 2.70 ms; inversion time = 950 ms; flip angle = 8°). The MRI scan was used for co-registration and for ROI definition.

PET data acquisition

All subjects underwent two identical PET scans on the same day. Scans were performed on an ECAT EXACT HR+ scanner (Siemens/CTI, Knoxville, USA), equipped with a neuro-insert to reduce the contribution of scattered photons from outside the field of view of the scanner. This scanner enables acquisition of 63 transaxial planes over a 15.5-cm axial field of view, allowing the whole brain to be imaged in a single bed position. The properties of this scanner have been reported elsewhere [26]. (*R*)-[^{11}C]verapamil was synthesised as described previously [27]. Prior to tracer injection a 10-min transmission scan in 2D acquisition mode was performed using three rotating ^{68}Ge rod sources. This scan was used to correct the subsequent emission scan for photon attenuation. Next, a dynamic emission scan in 3D acquisition mode was started simultaneously with an intravenous injection of approximately 370 MBq (*R*)-[^{11}C]verapamil. (*R*)-[^{11}C]verapamil was injected at a rate of

0.8 mL·s^{-1}, followed by a flush of 42 mL saline at 2.0 mL·s^{-1} using an infusion pump (Med-Rad, Beek, The Netherlands). The emission scan consisted of 20 frames with progressive increase in frame duration (1 x 15, 3 x 5, 3 x 10, 2 x 30, 3 x 60, 2 x 150, 2 x 300, 4 x 600 s) and a total scan duration of 60 min. During the (*R*)-[^{11}C]verapamil scan, arterial blood was withdrawn continuously using an automatic on-line blood sampler (Veenstra Instruments, Joure, The Netherlands [28]) at a rate of 5 mL·min^{-1} for the first 5 min and 2.5 mL·min^{-1} thereafter. At 2.5, 5, 10, 20, 30, 40 and 60 min after tracer injection, continuous blood sampling was interrupted briefly to withdraw a 10-mL manual blood sample, followed by flushing of the arterial line with a heparinised saline solution. These manual samples were used to determine plasma to whole blood (P/WB) radioactivity concentrations. In addition, concentrations of radioactive parent tracer and its polar metabolites in plasma were determined using a combination of solid-phase extraction and high-performance liquid chromatography, as described previously [29]. Patient movement was restricted by the use of a head holder and monitored by checking the position of the head using laser beams.

PET data analysis

All PET data were corrected for attenuation, randoms, dead time, scatter and decay. Images were reconstructed using a standard filtered back projection (FBP) algorithm, applying a Hanning filter with a cutoff at 0.5 times the Nyquist frequency. A zoom factor of 2.123 and a matrix size of 256 x 256 x 63 were used, resulting in a voxel size of 1.2 x 1.2 x 2.4 mm and a spatial resolution of approximately 6.5 mm full width at half maximum at the centre of the field of view. Images were also reconstructed using a partial volume corrected ordered subset expectation maximization (PVC OSEM) reconstruction algorithm, a previously described and validated method that results in improved image resolution, thereby reducing partial volume effects (PVEs) [30-32]. Co-registration of structural T1 MRI images with corresponding summed FBP or PVC OSEM reconstructed (*R*)-[^{11}C]verapamil images (frames 3 to 12) and segmentation of co-registered MRI images into grey matter, white matter and extracellular fluid was performed using statistical parametrical mapping (SPM, version SPM2, www.fil.ion.ucl.ac.uk/spm, Institute of Neurology, London, UK) software. ROIs were defined on the segmented MRI using a probabilistic template as implemented in the PVElab software [33]. The following ROIs were used for further analysis: frontal (volume weighted average of orbital frontal, medial inferior frontal and superior frontal), parietal, temporal (volume weighted average of superior temporal and medial inferior temporal), occipital, posterior and anterior cingulate, medial temporal lobe (MTL) (volume weighted average of hippocampus and enthorinal) and cerebellum. In addition, a global cortical region was defined consisting of the volume weighted average of frontal, parietal, temporal and occipital cortices, and posterior and anterior cingulate regions. ROIs were mapped onto dynamic PET images and regional time-activity curves (TACs) were generated.

The on-line blood curve was calibrated using the seven manual whole blood samples. Next, the total plasma curve was obtained by multiplying this calibrated whole blood curve with a single-exponential function derived from the best fit to the P/WB ratios. Finally, the corrected plasma input function was generated by multiplying this total plasma curve with a sigmoid function derived from the best fit to one minus the polar fraction [19,34].

Kinetic analyses of (*R*)-[^{11}C]verapamil data were performed using software developed within Matlab 7.04 (The Mathworks, Natick, MA, USA). Data were analysed using different compartment models, schematically shown in Figure 2.1, and for different outcome measures, which have been proposed in previous studies as methods for analysing (*R*)-[^{11}C] verapamil data. First, (*R*)-[^{11}C]verapamil data were analysed using non-linear regression to a standard single-tissue compartment model covering both the entire 60 min (1T2k^{60}) and only the first 10 min (1T2k^{10}) of data collection, yielding K_1, k_2, volume of distribution V_T and the fractional blood volume V_B. In addition, standard two-tissue compartment models without (2T4k) and with fixing K_1/k_2 to the mean whole brain grey matter value (2T4k^{VTnsfix}) were tested, yielding, in addition to the individual rate constants K_1 to k_4 and V_B, the outcome measures V_T and non-displaceable binding potential BP_{ND}. Goodness of fits for the various models was assessed by means of the Akaike information criterion (AIC) [35].

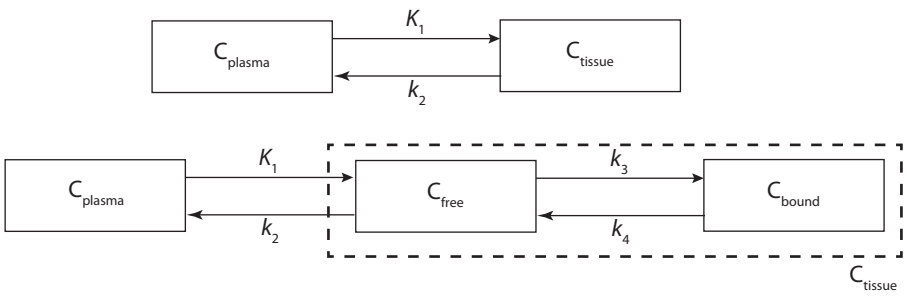

Figure 2.1 | Schematic diagrams of the compartment models.
In the upper diagram, a standard single-tissue compartment (1T2k) model is shown. In this study, two different implementations were used: the 1T2k^{60} model using 60 min of data acquisition and the 1T2k^{10} model using the first 10 min of data acquisition.
In the lower diagram a standard two-tissue compartment (2T4k) model is shown. In this study, two different implementations were used: the 2T4k model without and the 2T4k^{VTnsfix} model with fixation of K_1/k_2 to the whole brain grey matter value. C: compartment.

Statistical analysis

P values for assessing differences in characteristics between test and retest scans were obtained using Students *t* tests. Test-retest variability was calculated as the absolute difference between test and retest scans divided by the mean of these two scans. Differences in TRT variability between FBP and PVC OSEM reconstructed data were assessed using paired *t* tests. Furthermore, the level of agreement between test and retest scans was assessed using Bland-Altman analysis [36]; the difference in values between both measurements was plotted against their mean. Data are presented as mean ± standard deviation, unless otherwise stated.

RESULTS

Thirteen test and retest scans were performed. There were no differences in injected dose (test 361 ± 29 MBq, retest 374 ± 24 MBq; p=0.23) and specific activity (test 44 ± 13 GBq·µmol^{-1}, retest 49 ± 16 GBq·µmol^{-1}; p=0.41) of (*R*)-[^{11}C]verapamil between test and retest scans.

Two data sets had to be excluded from further analysis due to incomplete blood data. In one retest scan, the polar and parent fractions of the last manual sample were missing due to technical problems. Another retest scan clearly had erroneous values for the polar fraction of the last 2 manual samples. For the 11 subjects included in the analyses, TRT variability for the parent fraction (mean parent fraction of sample 6 and 7 at 40 and 60 min, respectively) ranged from 2% to 26% in individual subjects, with a mean of 13 ± 8%.

First, fits to the various models for the global cortical region were assessed using AIC. The 1T2k^{10} model was excluded from this analysis as it covers only 10 min rather than the entire 60 min of data acquisition. Since the 1T2k^{10} model differs in the number of data points (fewer frames and shorter scan duration) from the other models, AIC values cannot be compared with the other models. For FBP reconstructed data, the 2T4k^{VTnsfix} model provided best fits in 19 out of 22 scans (86%) according to the AIC with a mean value of -98 ± 13. The 1T2k^{60} and 2T4k models provided best fits in 1 (5%) and 2 (9%) out of 22 scans with mean AIC values of -81 ± 13 and -96 ± 14, respectively. Examples of the various model fits are shown in Figure 2.2. Similar results were obtained for PVC OSEM reconstructed PET data, with the lowest AIC (-103 ± 11) for the 2T4k^{VTnsfix} model in 17 out of 22 scans (77%). The 1T2k^{60} model (mean AIC value -88 ± 13) and 2T4k model (mean AIC value -101 ± 11) provided best fits in 2 (9%) and 3 (14%) out of 22 scans, respectively.

Table 2.1 summarizes TRT variability of the various outcome measures and parameters derived from FBP reconstructed (*R*)-[^{11}C]verapamil data for all ROIs investigated. Average TRT variability of 1T2k^{60} derived V_T for the global cortical brain region was 6.2% and regional TRT variability ranged from 5.8% in the occipital to 8.3% in the posterior cingulate region. Corresponding TRT variabilities of the rate constants K_1 and k_2 for the global cortical region were 9.1 and 10.0%, respectively. Regional data are summarised in Table 2.2.

For the 1T2k[10] model, TRT variability of the outcome measure K_1 was 8.8% for the global cortical ROI and varied from 8.6% in both temporal and occipital regions to 12.7% in the medial temporal lobe region (Table 2.1). Corresponding TRT values for V_T and k_2 are listed in Table 2.2.

The standard 2T4k model resulted in outcome measures and rate constants that could not be determined reliably (i.e. very high standard errors (SEs) of fitted parameters). Therefore, assessment of TRT variability did not seem useful. SEs of outcome parameters from the other models were very acceptable. For example, for the global cortical region and FBP reconstructed data, SE values were in the range of 0.14% for V_T (1T2k[60]), 2.7% for K_1 (1T2k[10]), 3.3% for V_T (2T4k^{VTnsfix}) and 3.2% for BP_{ND} (2T4k^{VTnsfix}).

For the 2T4k^{VTnsfix} model, TRT variability of the outcome measure BP_{ND} for the global cortical brain region was 22.0%, and regional TRT values varied from 22.5% in the occipital to 29.8% in the posterior cingulate region (Table 2.1). Corresponding TRT variability of V_T for the global cortical region was 8.9% (Table 2.1). TRT values of the rate constants K_1 to k_4 for the 2T4k^{VTnsfix} model are given in Table 2.2.

Tables 2.3 and 2.4 provide similar data as Tables 2.1 and 2.2, but now for PVC OSEM rather than FBP reconstructed data. Although there was some regional variation, TRT variability of all parameters derived from all models was comparable, though not exactly the same as for FBP reconstructed data. Although TRT variabilities of K_1 obtained with the 1T2k[10] model, and BP_{ND} and V_T obtained with the 2T4k^{VTnsfix} model were slightly higher for PVC OSEM reconstructed data, these differences between both reconstruction methods were not statistically significant (tested using paired *t* tests) for any of the regions assessed. Next, the level of agreement between test and retest scans was assessed by plotting the difference in values between both measurements against their mean for the various outcome measures, as shown in Figure 2.3.

Table 2.1 | Test-retest variability (%) of various outcome measures of (R)-[^{11}C]verapamil kinetics derived from filtered back projection data.

	1T2k[60] V_T	**1T2k[10]** K_1	**2T4k^{VTnsfix}** BP_{ND}	**2T4k^{VTnsfix}** V_T
Global	6.2 ± 4.0	8.8 ± 6.4	22.0 ± 29.6	8.9 ± 6.8
Frontal	6.2 ± 3.9	9.1 ± 6.6	22.9 ± 27.8	9.6 ± 7.1
Parietal	6.0 ± 4.3	9.1 ± 5.5	22.9 ± 28.0	10.2 ± 7.5
Temporal	6.8 ± 4.1	8.6 ± 6.1	22.9 ± 29.7	7.9 ± 6.7
Occipital	5.8 ± 4.7	8.6 ± 7.6	22.5 ± 27.4	11.0 ± 7.4
Posterior Cingulate	8.3 ± 6.0	11.1 ± 8.8	29.8 ±37.0	13.6 ± 8.8
Anterior Cingulate	7.0 ± 5.8	10.5 ± 5.7	27.6 ± 30.9	9.8 ± 7.4
Medial Temporal	7.8 ± 5.0	12.7 ± 9.6	25.5 ± 25.0	11.5 ± 6.2
Cerebellum	6.8 ± 6.6	10.4 ± 7.8	25.3 ± 27.0	13.2 ± 11.2

Figure 2.2 | Examples of various fits.

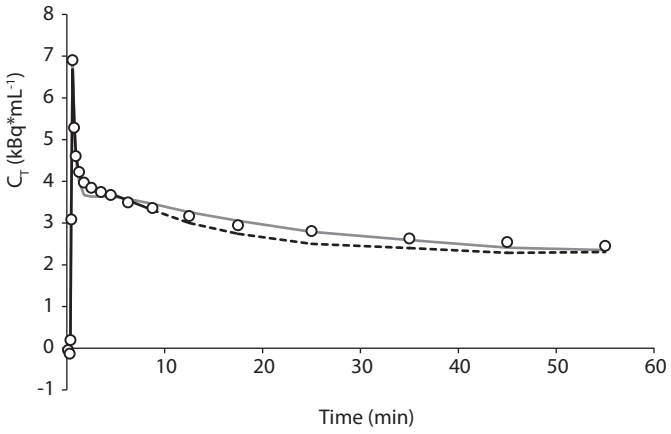

A | The standard single-tissue compartment models fitted to the entire 60 min (1T2k^{60}, grey line) and only to the first 10 min (1T2k^{10}, black line) of data collection. The dashed black line represents an extrapolation of the 1T2k^{10} fit, i.e. data from 10 to 60 min were not used for fitting.

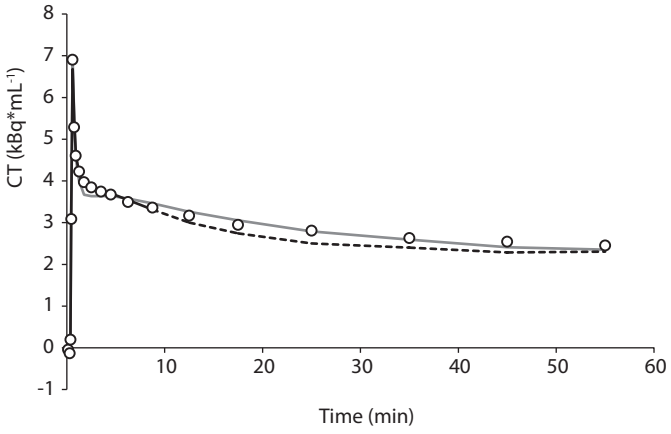

B | Fits obtained with the standard single-tissue compartment model (1T2k^{60}, grey line) and the two-tissue compartment model with fixed K_1/k_2 (2T4k^{VTnsfix}, black line). Fits of the unconstrained (standard) two-tissue compartment model (2T4k) were identical to those of the 2T4k^{VTnsfix} model.

Table 2.2 | Test-retest variability (%) of various (*R*)-[^{11}C]verapamil rate constants derived from filtered back projection reconstructed data.

	1T2k^{60} K_1	1T2k^{60} k_2	1T2k^{10} V_T	1T2k^{10} k_2	2T4k^{VTnsfix} K_1	2T4k^{VTnsfix} k_2	2T4k^{VTnsfix} k_3	2T4k^{VTnsfix} k_4
Global	9.1 ± 7.0	10.0 ± 6.0	5.9 ± 5.9	9.2 ± 5.1	9.1 ± 7.0	19.2 ± 27.1	66.2 ± 56.4	60.6 ± 45.0
Frontal	10.2 ± 6.7	10.3 ± 5.7	6.9 ± 6.3	9.2 ± 5.7	10.0 ± 6.4	19.6 ± 27.1	63.3 ± 56.1	58.5 ± 45.9
Parietal	9.4 ± 7.1	11.2 ± 6.0	6.9 ± 5.3	8.1 ± 7.1	9.2 ± 7.5	18.4 ± 27.0	63.1 ± 55.8	61.0 ± 45.3
Temporal	8.0 ± 6.4	8.9 ± 6.5	6.8 ± 5.3	11.3 ± 5.9	10.1 ± 6.3	20.1 ± 26.5	75.7 ± 57.3	65.7 ± 47.9
Occipital	9.7 ± 8.1	10.6 ± 5.0	6.6 ± 6.5	8.3 ± 4.9	8.3 ± 9.5	19.3 ± 28.8	68.8 ± 66.1	66.8 ± 59.1
Posterior Cingulate	9.9 ± 10.3	9.5 ± 7.8	14.1± 14.4	16.8 ± 14.1	9.8 ± 8.3	21.1 ± 25.8	77.9 ± 65.4	73.7 ± 55.1
Anterior Cingulate	9.7 ± 6.7	11.6 ± 6.6	16.7 ± 15.7	20.7 ± 18.1	10.2 ± 6.3	17.8 ± 25.5	71.0 ± 65.9	71.6 ± 54.5
Medial Temporal	10.6 ± 9.3	11.1 ± 9.5	16.8 ± 12.6	25.1 ± 15.3	13.0 ± 8.1	22.7 ± 27.6	69.7 ± 39.5	60.6 ± 40.3
Cerebellum	10.9 ± 7.6	10.3 ± 6.7	6.8 ± 4.8	7.2 ± 5.7	10.2 ± 7.9	18.6 ± 27.0	58.1 ± 55.6	61.4 ± 44.1

Table 2.4 | Test-retest variability (%) of various (*R*)-[^{11}C]verapamil rate constants derived from PVC OSEM reconstructed data.

	1T2k^{60} K_1	1T2k^{60} k_2	1T2k^{10} V_T	1T2k^{10} k_2	2T4k^{VTnsfix} K_1	2T4k^{VTnsfix} k_2	2T4k^{VTnsfix} k_3	2T4k^{VTnsfix} k_4
Global	9.9 ± 8.0	10.2 ± 7.2	7.4 ± 7.3	9.7 ± 6.3	8.2 ± 6.5	21.9 ± 26.1	62.2 ± 54.4	50.2 ± 38.2
Frontal	10.1 ± 7.9	10.4± 8.0	9.3 ± 9.2	11.1 ± 7.7	7.6 ± 5.1	21.3 ± 25.1	61.5 ± 57.8	51.0 ± 43.6
Parietal	10.7 ± 8.1	11.3 ± 6.9	9.0 ± 5.9	11.5 ± 9.9	9.7 ± 7.8	22.9 ± 26.0	66.1 ± 57.5	57.7 ± 40.2
Temporal	9.1 ± 8.2	11.6 ± 6.8	7.1 ± 5.8	9.4 ± 6.2	8.0 ± 7.2	22.2 ± 26.1	61.7 ± 52.6	49.3 ± 36.1
Occipital	11.0 ± 7.6	9.3 ± 7.1	6.7 ± 7.5	9.7 ± 6.7	10.7 ± 7.5	23.1 ± 28.8	60.0 ± 56.1	49.1 ± 39.1
Posterior Cingulate	13.4 ± 11.5	11.4 ± 8.2	15.6 ± 10.1	17.7 ± 9.5	13.6 ± 10.6	28.0 ± 27.4	84.4 ± 57.1	69.8 ± 54.1
Anterior Cingulate	12.9 ± 9.3	12.6 ± 8.8	13.8 ± 8.6	21.7 ± 12.5	11.3 ± 6.2	23.3 ± 24.6	74.7 ± 63.8	65.4 ± 50.7
Medial Temporal	15.0 ± 21.7	14.4 ± 13.0	25.8 ± 13.2	38.3 ± 22.1	16.9 ± 19.1	28.6 ± 31.1	82.3 ± 53.5	79.2 ± 45.5
Cerebellum	8.4 ± 7.5	10.2 ± 6.8	10.1 ± 6.4	10.6 ± 6.7	7.2 ± 5.9	20.8 ± 26.1	68.0 ± 60.8	59.1 ± 47.5

Table 2.3 | Test-retest variability (%) of various outcome measures of (*R*)-[^{11}C]verapamil kinetics derived from PVC OSEM reconstructed data.

	1T2k^{60} V_T	1T2k^{10} K_1	2T4k^{VTnsfix} BP_{ND}	2T4k^{VTnsfix} V_T
Global	6.3 ± 4.7	9.6 ± 6.7	22.7 ± 32.2	9.0 ± 6.2
Frontal	6.4 ± 4.8	9.2 ± 6.2	24.7 ± 30.0	9.0 ± 7.1
Parietal	5.7 ± 3.7	10.6 ± 7.1	23.3 ± 31.0	9.4 ± 5.7
Temporal	7.2 ± 4.9	9.3 ± 6.6	25.8 ± 30.9	9.2 ± 6.4
Occipital	6.8 ± 6.1	10.8 ± 7.4	23.2 ± 32.1	10.0 ± 7.2
Posterior Cingulate	9.3 ± 6.9	13.3 ± 10.1	33.5 ± 37.4	13.1 ± 8.8
Anterior Cingulate	5.9 ± 5.2	14.2 ± 5.8	28.5 ± 34.2	8.5 ± 5.4
Medial Temporal	11.8 ± 10.8	18.9 ± 23.1	38.8 ± 32.5	18.6 ± 19.9
Cerebellum	6.3 ± 4.5	7.6 ± 5.6	26.2 ± 30.9	10.6 ± 6.1

DISCUSSION

This study evaluated test-retest variability of (*R*)-[^{11}C]verapamil data using several tracer kinetic models. Of the three outcome measures that have been suggested to reflect Pgp function, the best TRT variability was found for V_T using the 1T2k^{60} model (global TRT 6%). Using the 2T4k^{VTnsfix} model, comparable TRT variability was found for V_T (global TRT 9%), but TRT variability for BP_{ND} was higher (global TRT 22%). For K_1 derived from the 1T2k^{10} model, global TRT variability was 9%. TRT variability could not be assessed for the 2T4k model without fixing K_1/k_2 to a global value. In a previous study evaluating several compartment models for (*R*)-[^{11}C]verapamil data, it has also been shown that TRT variability was substantially higher for a 2T4k model, and in that study, it was concluded that the 1T2k model was the model of choice for analysing (*R*)-[^{11}C]verapamil data [19]. Nevertheless, in this study, AIC analysis showed that the 2T4k^{VTnsfix} model provided better fits to the data than the standard single-tissue compartment model, with substantial differences in AIC values. Furthermore, test-retest variability and precision of the fitted outcome measures were very acceptable. Regarding the 1T2k^{10} model as proposed by Muzi et al., TRT variability of the outcome measure K_1 was moderate, the quality of the fit (over the first 10 min) was good and a shorter scan duration is an advantage, especially in certain patient groups. Nevertheless, K_1 might not fully reflect Pgp function. Although a significant increase in K_1 was found after Pgp inhibition, there was an even larger increase in k_3 [23]. In addition, previous studies as well as spectral analysis have shown that there are two compartments in (*R*)-[^{11}C]verapamil data, in healthy controls under baseline conditions, in Alzheimer's disease patients [9] and especially after pharmacological blockade of Pgp [21,23]. Therefore, despite its slightly higher TRT of V_T, the 2T4k^{VTnsfix} is the tracer kinetic model of choice, even for baseline studies in healthy controls. Although TRT variability of BP_{ND} was higher, TRT

Figure 2.3 | Bland-Altman plots for the various outcome measures derived from FBP and PVC OSEM reconstructed data. (A) 1T2k model, V_T as outcome measure. (B) 1T2k[10] model, K_1 as outcome measure. (C) 2T4k[VTnsfix] model, BP_{ND} as outcome measure. The Greek letter delta represenst the change between test and retest values in the global cortical region. On the *x*-axis the mean of test and retest values is given. Squares: FBP data; triangles: PVC OSEM data.

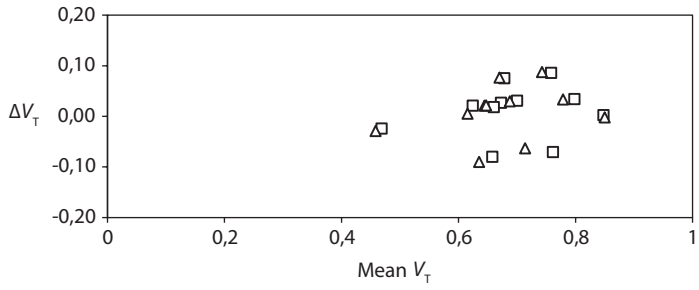

A | 1T2k model, V_T as outcome measure.

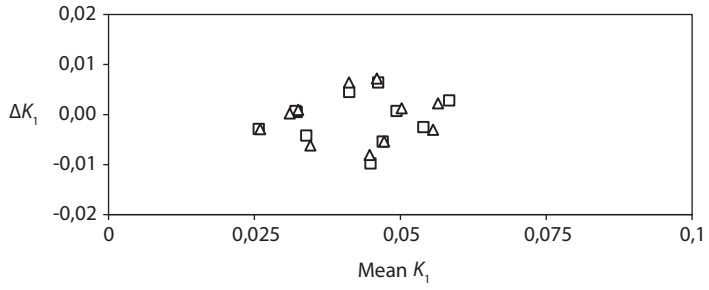

B | 1T2k[10] model, K_1 as outcome measure.

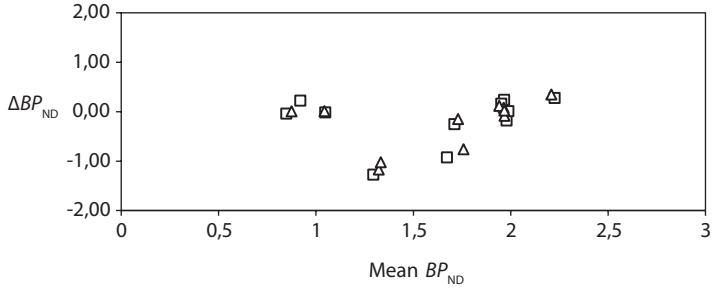

C | 2T4k[VTnsfix] model, BP_{ND} as outcome measure.

Figure 2.4 | Test-retest variability (TRT %) as function of ROI volume. (A) FBP reconstructed data and (B) PVC OSEM reconstructed data. Squares: 1T2k^{60} model with outcome measure V_T; triangles: 1T2k^{10} model with outcome measure K_1; circles: 2T4k^{VTnsfix} model with outcome measure BP_{ND}; crosses: 2T4k^{VTnsfix} model with outcome measure V_T.

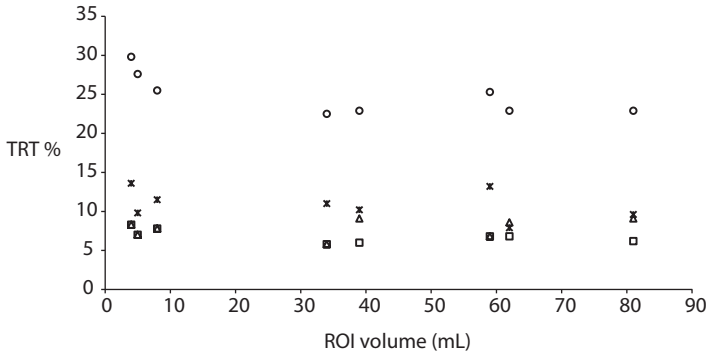

A | FBP reconstructed data.

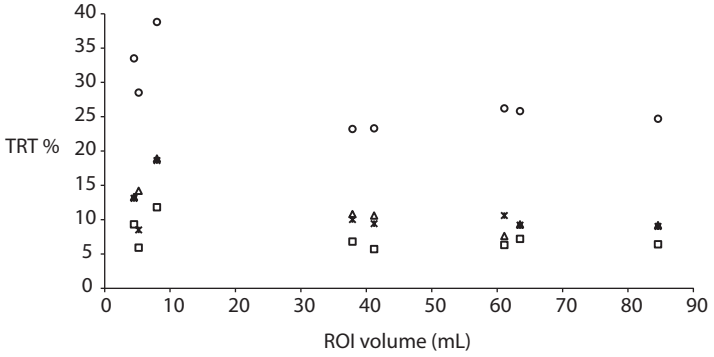

B | PVC OSEM reconstructed data.

variability of V_T was quite similar for the constrained two-tissue and standard single-tissue compartment models. Therefore, V_T derived from the constrained two-tissue compartment model should be used. This has the further advantage that the same model can be used in blocking experiments, where baseline scans are compared with scans after administration of a Pgp inhibitor, or when comparing different groups of patients.

The present study is the first to assess TRT variability of regional (*R*)-[^{11}C]verapamil data, as previous studies have reported on total brain TRT variability only [19]. Although there is a slight decrease (approximately 5%) in reproducibility for brain regions with the smallest volumes, such as the anterior and posterior cingulate, this effect is only marginal (Figure

4). The slightly higher TRT values in the medial temporal lobe (Tables 2.1 and 2.3) may be secondary to spill over from the very high signal in the choroid plexus.

The effect of PVE correction methods on TRT variability of (*R*)-[^{11}C]verapamil data has not been assessed before. In the present study, images were reconstructed using both standard FBP and PVC OSEM reconstruction algorithms [30]. PVC OSEM improves in-plane resolution of PET images by taking the point spread function of the scanner into account, leading to reduced PVEs [31]. Interestingly, differences in TRT variability between PVC OSEM and FBP reconstructed data were only minor (Tables 2.1 and 2.3). It should, however, be noted that only healthy controls were included and, although the age range varied from 21 to 63 years, there was no significant brain atrophy present on MRI scans. The effects of PVE correction methods and their impact on TRT variability should be assessed in future studies in conditions where brain atrophy may be present, such as in neurodegenerative diseases. However, as (*R*)-[^{11}C]verapamil is a tracer which has low uptake throughout the brain and therefore shows little contrast, no major effects from PVE correction methods should be expected. Even in the medial temporal lobe, where the signal was higher than in other brain regions, no improvement in TRT variability was seen. In fact, TRT variability in this region was higher after PVE correction. For MTL, PVE correction implies a small signal following a large correction for PVEs. Consequently, noise levels in the corrected MTL signal will be higher than in other regions, resulting in higher TRT values.

In conclusion, reproducibility of (*R*)-[^{11}C]verapamil PET studies was best for V_T derived from single-tissue (6%) and constrained two-tissue (9%) compartment models. As the constrained two-tissue compartment model provided the best fits to the data, it is the kinetic model of choice with the volume of distribution V_T as preferred outcome measure.

Acknowledgements

The authors would like to thank the radiochemistry and technology staff of the Department of Nuclear Medicine & PET Research for tracer production and acquisition of PET data, respectively. In addition, staff of the Department of Radiology is acknowledged for acquisition of MRI data.

The research leading to these results has received funding from the European Community's Seventh Framework Programme (FP7/2007-2013) under grant agreement n° 201380.

REFERENCES

1. Schinkel AH. P-Glycoprotein, a gatekeeper in the blood-brain barrier. *Adv Drug Deliv Rev* 1999;36:179-194.
2. Demeule M, Labelle M, Regina A, Berthelet F, Beliveau R. Isolation of endothelial cells from brain, lung, and kidney: expression of the multidrug resistance P-glycoprotein isoforms. *Biochem Biophys Res Commun* 2001;281:827-834.
3. Fromm MF. Importance of P-glycoprotein at blood-tissue barriers. *Trends Pharmacol Sci* 2004;25:423-429.
4. de Lange EC. Potential role of ABC transporters as a detoxification system at the blood-CSF barrier. *Adv Drug Deliv Rev* 2004;56:1793-1809.
5. Loscher W, Potschka H. Blood-brain barrier active efflux transporters: ATP-binding cassette gene family. *NeuroRx* 2005;2:86-98.
6. Vogelgesang S, Cascorbi I, Schroeder E, Pahnke J, Kroemer HK, Siegmund W, Kunert-Keil C, Walker LC, Warzok RW. Deposition of Alzheimer's beta-amyloid is inversely correlated with P-glycoprotein expression in the brains of elderly non-demented humans. *Pharmacogenetics* 2002;12:535-541.
7. Vogelgesang S, Glatzel M, Walker LC, Kroemer HK, Aguzzi A, Warzok RW. Cerebrovascular P-glycoprotein expression is decreased in Creutzfeldt-Jakob disease. *Acta Neuropathol* 2006;111:436-443.
8. Bartels AL, Willemsen AT, Kortekaas R, de Jong BM, de VR, de KO, van Oostrom JC, Portman A, Leenders KL. Decreased blood-brain barrier P-glycoprotein function in the progression of Parkinson's disease, PSP and MSA. *J Neural Transm* 2008;115:1001-1009.
9. van Assema DM, Lubberink M, Bauer M, van der Flier WM, Schuit RC, Windhorst AD, Comans EF, Hoetjes NJ, Tolboom N, Langer O, Muller M, Scheltens P, Lammertsma AA, van Berckel BN. Blood-brain barrier P-glycoprotein function in Alzheimer's disease. *Brain* 2012;135:181-189.
10. Langer O, Bauer M, Hammers A, Karch R, Pataraia E, Koepp MJ, Abrahim A, Luurtsema G, Brunner M, Sunder-Plassmann R, Zimprich F, Joukhadar C, Gentzsch S, Dudczak R, Kletter K, Muller M, Baumgartner C. Pharmacoresistance in epilepsy: a pilot PET study with the P-glycoprotein substrate R-[(11)C]verapamil. *Epilepsia* 2007;48:1774-1784.
11. Bartels AL, van Berckel BN, Lubberink M, Luurtsema G, Lammertsma AA, Leenders KL. Blood-brain barrier P-glycoprotein function is not impaired in early Parkinson's disease. *Parkinsonism & Related Disorders* 2008;14:505-508.
12. Bauer M, Karch R, Neumann F, Abrahim A, Wagner CC, Kletter K, Muller M, Zeitlinger M, Langer O. Age dependency of cerebral P-gp function measured with (R)-[11C]verapamil and PET. *Eur J Clin Pharmacol* 2009;65:941-946.
13. Kreisl WC, Liow JS, Kimura N, Seneca N, Zoghbi SS, Morse CL, Herscovitch P, Pike VW, Innis RB. P-glycoprotein function at the blood-brain barrier in humans can be quantified with the substrate radiotracer 11C-N-desmethyl-loperamide. *J Nucl Med* 2010;51:559-566.
14. Seneca N, Zoghbi SS, Liow JS, Kreisl W, Herscovitch P, Jenko K, Gladding RL, Taku A, Pike VW, Innis RB. Human brain imaging and radiation dosimetry of 11C-N-desmethyl-loperamide, a PET radiotracer to measure the function of P-glycoprotein. *J Nucl Med* 2009;50:807-813.
15. Kannan P, John C, Zoghbi SS, Halldin C, Gottesman MM, Innis RB, Hall MD. Imaging the function of P-glycoprotein with radiotracers: pharmacokinetics and in vivo applications. *Clin Pharmacol Ther* 2009;86:368-377.
16. Syvanen S, Hammarlund-Udenaes M. Using PET studies of P-gp function to elucidate mechanisms underlying the disposition of drugs. *Curr Top Med Chem* 2010;10:1799-1809.
17. Vogelgesang B, Echizen H, Schmidt E, Eichelbaum M (2004). Stereoselective first-pass metabolism of highly cleared drugs: studies of the bioavailability of L- and D-verapamil examined with a stable isotope technique. *Br J Clin Pharmacol* 1984;58:S796-S803.
18. Toornvliet R, van Berckel BN, Luurtsema G, Lubberink M, Geldof AA, Bosch TM, Oerlemans R, Lammertsma AA, Franssen EJ. Effect of age on functional P-glycoprotein in the blood-brain barrier measured by use of (R)-[(11)C]verapamil and positron emission tomography. *Clin Pharmacol Ther* 2006;79:540-548.
19. Lubberink M, Luurtsema G, van Berckel BN, Boellaard R, Toornvliet R, Windhorst AD, Franssen EJ, Lammertsma AA. Evaluation of tracer kinetic models for quantification of P-glycoprotein function using (R)-[11C]verapamil and PET. *J Cereb Blood Flow Metab* 2007;27:424-433.

20. Bartels AL, Kortekaas R, Bart J, Willemsen AT, de Klerk OL, de Vries JJ, van Oostrom JC, Leenders KL. Blood-brain barrier P-glycoprotein function decreases in specific brain regions with aging: a possible role in progressive neurodegeneration. *Neurobiol Aging* 2009;30:1818-1824.
21. Wagner CC, Bauer M, Karch R, Feurstein T, Kopp S, Chiba P, Kletter K, Loscher W, Muller M, Zeitlinger M, Langer O. A pilot study to assess the efficacy of tariquidar to inhibit P-glycoprotein at the human blood-brain barrier with (R)-11C-verapamil and PET. *J Nucl Med* 2009;50:1954-1961.
22. Bauer M, Karch R, Neumann F, Wagner CC, Kletter K, Muller M, Loscher W, Zeitlinger M, Langer O. Assessment of regional differences in tariquidar-induced P-glycoprotein modulation at the human blood-brain barrier. *J Cereb Blood Flow Metab* 2010;30:510-515.
23. Muzi M, Mankoff DA, Link JM, Shoner S, Collier AC, Sasongko L, Unadkat JD. Imaging of cyclosporine inhibition of P-glycoprotein activity using 11C-verapamil in the brain: studies of healthy humans. *J Nucl Med* 2009;50:1267-1275.
24. Bart J, Groen HJ, Hendrikse NH, van der Graaf WT, Vaalburg W, de Vries EG. The blood-brain barrier and oncology: new insights into function and modulation. *Cancer Treat Rev* 2000;26:449-462.
25. Didziapetris R, Japertas P, Avdeef A, Petrauskas A. Classification analysis of P-glycoprotein substrate specificity. *J Drug Target* 2003;11:391-406.
26. Brix G, Zaers J, Adam LE, Bellemann ME, Ostertag H, Trojan H, Haberkorn U, Doll J, Oberdorfer F, Lorenz WJ. Performance evaluation of a whole-body PET scanner using the NEMA protocol. National Electrical Manufacturers Association. *J Nucl Med* 1997;38:1614-1623.
27. Luurtsema G, Windhorst AD, Mooijer MP, Herscheid JD, Lammertsma AA, Franssen EJ. Fully automated high yield synthesis of (R)- and (S)-[C-11]verapamil for measuring P-glycoprotein function with positron emission tomography. *J Labelled Compds Radiopharm* 2002;45:1199-1207.
28. Boellaard R, van LA, van Balen SC, Hoving BG, Lammertsma AA. Characteristics of a new fully programmable blood sampling device for monitoring blood radioactivity during PET. *Eur J Nucl Med* 2001;28:81-89.
29. Luurtsema G, Molthoff CF, Schuit RC, Windhorst AD, Lammertsma AA, Franssen EJ. Evaluation of (R)-[11C]verapamil as PET tracer of P-glycoprotein function in the blood-brain barrier: kinetics and metabolism in the rat. *Nucl Med Biol* 2005;32:87-93.
30. Mourik JE, Lubberink M, Klumpers UM, Comans EF, Lammertsma AA, Boellaard R. Partial volume corrected image derived input functions for dynamic PET brain studies: methodology and validation for [11C]flumazenil. *Neuroimage* 2008;39:1041-1050.
31. Brix G, Doll J, Bellemann ME, Trojan H, Haberkorn U, Schmidlin P, Ostertag H. Use of scanner characteristics in iterative image reconstruction for high-resolution positron emission tomography studies of small animals. *Eur J Nucl Med* 1997;24:779-786.
32. Mourik JE, Lubberink M, van Velden FH, Kloet RW, van Berckel BN, Lammertsma AA, Boellaard R. In vivo validation of reconstruction-based resolution recovery for human brain studies. *J Cereb Blood Flow Metab* 2010;30:381-389.
33. Svarer C, Madsen K, Hasselbalch SG, Pinborg LH, Haugbol S, Frokjaer VG, Holm S, Paulson OB, Knudsen GM. MR-based automatic delineation of volumes of interest in human brain PET images using probability maps. *Neuroimage* 2005;24:969-979.
34. Gunn RN, Sargent PA, Bench CJ, Rabiner EA, Osman S, Pike VW, Hume SP, Grasby PM, Lammertsma AA. Tracer kinetic modeling of the 5-HT1A receptor ligand [carbonyl-11C]WAY-100635 for PET. *Neuroimage* 1998;8:426-440.
35. Akaike H. A new look at the statistical model indentification. *IEEE Trans Autom Contr* 1974;716-723.
36. Bland JM, Altman DG. Statistical methods for assessing agreement between two methods of clinical measurement. *Lancet* 1986;1:307-310.